Toward 3D UWB Tomographic Imaging System for Breast Tumor Detection

M. Guardiola*, L. Jofre*, S. Capdevila*, S. Blanch*, J. Romeu*
*AntennaLab, Universitat Politècnica de Catalunya
C/ Jordi Girona 3-4 building D3, 08034 Barcelona (Spain)
{marta.guardiola, jofre, scapdevila, blanch, romeu}@.tsc.upc.edu

***Abstract*—A novel 3D tomographic algorithm for short range cylindrical geometries using UWB frequency range is presented. The algorithm has been applied to breast tumor detection, nevertheless, its non application-specific character permits the use in other applications. The detection capability of the tomographic algorithm is proved through numerical simulations and experimental measurements of canonical and more realistic body-attached breast phantoms. For the acquisition of the experimental data, a virtual array-based cylindrical measurement setup has been built. At the current stage of development 3 degrees of freedom are available allowing the scanning of bodies with revolution symmetry.**

I. Introduction

Breast cancer is recognized as a severe public health problem provided by its high incidence rate. Recent studies [1] reported that it is the most common form of cancer in Europe, with 429 900 cases (13.5% of all cancer causes) and the third most common cause of death form cancer (131 900 deaths). Early stage detection has demonstrated to increase significantly the survival rates, motivating the uprising of new imaging solutions. Active microwave imaging has been developed rapidly over the last two decades, as an alternative to the well-established, but not exempt from problems, X-ray mammography method. The potential for microwave imaging for practical clinical use is significant, due to a wide variety of advantages, such as low-cost system implementation, the use of low-power, non-ionizing radiation, patient comfort and promising initial clinical investigations. However, the most recently published data on electromagnetic properties of breast tissues [2] suggest that the contrast between healthy and malignant tissues might be significantly lower than indicated by previously published data. This poses a challenge for reconstruction algorithms and show that there is still room for more research into this topic.

Up to now, active microwave imaging techniques were mainly developed for 2D configurations either by using tomographic [3], confocal [4], or multi-physics [5] approaches. In the framework of microwave tomography, an inverse scattering problem has to be solved to retrieve the dielectric properties of tissues form the measured scattered fields. Many research groups are focused in iterative algorithms to deal with such undetermined problems. Nevertheless, many times they require to introduce a priori information about the imaged tissue by assuming any property as known [6], becoming application-specific and in the worst scenario, badly pre-conditioning the solution. Additionally, they are in general computationally intensive. On the other hand, linearizing approximations, such as Born approximation, on which the method proposed here is partially based [3], allows to obtain reconstructions with a reasonable error, in a very efficient way and without requiring a priori information, being however limited to small low-contrast objects due to the residual phase errors produced by the non-object induced field supposition. When trying to combine these images comprising residual phase errors into a multi-frequency system, a strong interference effect appear producing important distortion into the final image. Thus in [7] and [8] an amplitude (phase-less) multi-frequency combination has been proposed to overcome this undesired effect.

Nowadays, there is an increasing interest in 3D reconstruction algorithms boosted by the advent of both efficient numerical approaches and more powerful PCs [9]. UWB radar based algorithms have been already used to obtain 3D reconstructions since they are inherently 3D, however up to now they remain limited by the inhomogeneity of the breast [10]. Tomographic approach is being also investigated specially using iterative schemes. As early as 1991, Newton-Kantorwich iterative algorithm was applied to a very simple 3D configuration in [11]. More recently, other iterative schemes were investigated in 3D configurations, as Gradient Method [12], Born Iterative Method [13], a full-vectorial 3D inversion method [14] and a 3D quantitative inversion method in time domain [15]. Nevertheless, due to the very high computational cost of both forward and inverse problems in 3D, most studies on iterative schemes have been limited to 2D. This opens the door to less computationally heavy algorithms as ones based on linearizing approximations.

In this paper, preliminary efforts directed to study the performance of the extension to 3D of the 2D UWB Hybrid Focusing algorithm are made. In first section, the algorithm is introduced and formulated. Next, reconstructions of numerical isolated and body attached simplified breast phantoms are included. Finally an embryonic measurement setup is described and first measurement results presented.

II. 3D UWB Hybrid Focusing Algorithm

3D UWB Hybrid focusing image reconstruction algorithm is based on previous work carried out in UPC on tomographic imaging algorithms for 2D circular geometries [3]. In [7], it has been extended to multi-frequency performance by using

UWB frequency range. In this paper, a new formulation for 3D cylindrical geometries is presented, see Fig. 1. The idea

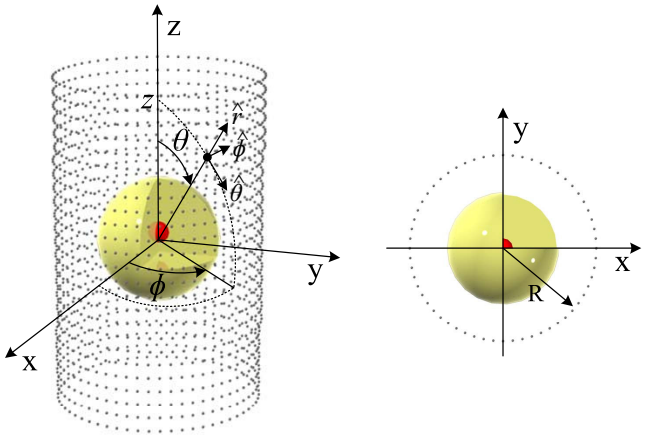

Fig. 1. 3D view and XY plane of the measurement geometry. In black the coordinate system for plane waves and the antenna position is represented.

under UWB Hybrid Focusing consists in the incoherent multi-frequency combination of coherent multi-view focused images. Its 2D version has demonstrated good detection capability even when electrically large and highly-contrasted objects, such as breasts, are scanned [7]. By using UWB frequency range, smoother reconstructions preserving better the aspect of the object under test and offering better clutter rejection when compared to mono-frequency approaches, can be retrieved.

A. 3D Cylindrical Tomographic Formulation

The tomographic algorithm here presented, relies on obtaining the dielectric contrast $C(\vec{r})$ of the scene, which is related to the complex permittivity of the body under test through:

$$C(\vec{r}) = 1 - \frac{\epsilon(\vec{r})}{\epsilon_0^{ext}} \tag{1}$$

where ϵ_0^{ext} is the permittivity of the external medium.

Using the reciprocity theorem (2), one can obtain the induced current on the object ($\vec{J}^b$), which is linked to the dielectric contrast, from the scattered field measured along the cylindrical antenna.

$$\int_{v_a} \vec{J}^a \vec{E}^b \mathrm{d}v_a = \int_{v_b} \vec{J}^b \vec{E}^a \mathrm{d}v_b \tag{2}$$

where $\vec{J}^a$ is the electric current on the antenna acting as a transmitter that radiates a plane wave electric field ($\vec{E}^a$) propagating along the vector $\vec{k}_2$. $\vec{J}^b$ is the electric current on the object that radiates the scattered field which is measured along the antenna and is induced by the plane wave incident field ($\vec{E}^b$) propagating along the vector $\vec{k}_1$. The direction of a plane wave propagating according to (θ, ϕ) is defined as follows:

$$\vec{k} = k_0^{ext}(cos\theta sin\phi\, \hat{x} + sin\theta sin\phi\, \hat{y} + cos\theta\, \hat{z}) \tag{3}$$

Under Born approximation (the scattered field is negligible in front of the incident field), the induced current $\vec{J}^b$ can be expressed as:

$$\vec{J}^b(\vec{r}) \cong j\omega\epsilon_0^{ext} C(\vec{r})\vec{E}^0(\vec{r};\vec{k}_1) \overset{\mathscr{F}}{\Rightarrow} \vec{J}(\vec{\eta}) \cong j\omega\epsilon_0^{ext}\tilde{C}(\vec{\eta} - \vec{k}_1) \tag{4}$$

For a cylindrical antenna, plane waves can be synthesized as the combination of cylindrical waves emanating from a number of probes. Accordingly, the amplitude to be applied to a probe situated at (θ', z') to produce a plane wave towards $\vec{k}$ [16] is:

$$I(\phi', z'; \vec{k}) = -\frac{1}{2\pi^2} e^{jk_z z'} \sum_{n=1}^{k_0 R} j^{n+1} e^{jn(\phi-\phi')} \frac{1}{sin\theta\, H_n^{(2)}(k_R R)} \tag{5}$$

where R is the radius of the cylindrical antenna, $k_z = k_0^{ext} cos\theta$ and $k_z = \sqrt{(k_0^{ext})^2 - k_z^2}$.

Finally, replacing (4) and (5) in (2), the spectrum of the contrast profile can be expressed as:

$$C(\vec{k}_1 + \vec{k}_2) = \frac{1}{j\omega\epsilon_0^{ext}} \sum_{i=1}^{N_T} \sum_{j=1}^{N_R} E^s(\phi'_{T_i}, z'_{T_i}; \phi'_{R_j}, z'_{R_j}) \\ I(\phi'_{T_i}, z'_{T_i}; \vec{k}_1) I(\phi'_{R_j}, z'_{R_j}; \vec{k}_2) \tag{6}$$

From equation 6 it can be seen that for a given frequency we obtain a sampled version of the spectrum of the contrast profile inside a sphere of radius k_0^{ext} and hence the reconstructed contrast profile will consist of a smoothed version of the original one. For a given transmitter, by measuring with a cylindrical array we will be sampling the spectrum of the contrast profile in an off-centered sphere. By doing so for a set of transmitters, the sampling will be in a sphere of radius $2k_0^{ext}$, see Fig. 2. Moreover, due to the limited extent of the measurement surface in the z direction, there is truncation error, which is translated as a deterioration of the synthesized plane wave. Furthermore, the closer θ is to 0°or 180°, the less accurate the plane wave is. Unacceptable plane waves may produce the degradation of the reconstruction. In order to prevent it happening, θ has been limited between 45°and 135°. In this way, an extra smoothing of the reconstruction is produced, but in any case, the detection of the reconstructed objects may not be affected, see Fig. 3

B. UWB Extension

The previous algorithm has been extended to UWB frequency range by pursuing an improvement of its performance with respect to mono-frequency case. By using information spanning in the whole UWB frequency range, we obtain a change of radius in the spectrum spheres, reverting in a wider and denser mesh of reconstruction. On the image, it is translated as an improvement of clutter rejection and a better recovering of the object appearance, as shown in [7]. In particular, higher frequencies give information about contours and lower frequencies contribute to the reconstruction of smoother parts as the inside of the breast.

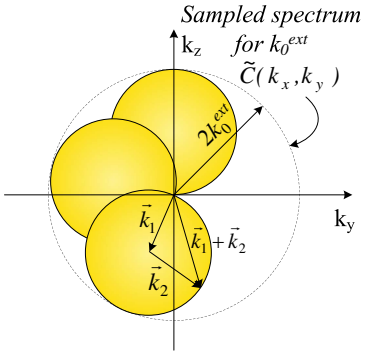

Fig. 2. By measuring with a circular array for a given transmitter, we will be sampling the dielectric contrast in a circle. By doing so for a set of transmitters the sampling will be inside an off-centered circle of radius $2k_0^{ext}$.

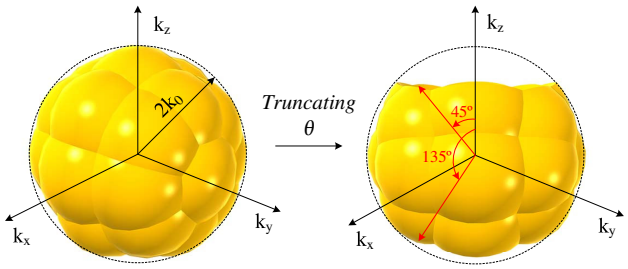

Fig. 3. When measuring with a cylindrical array the sampling will be inside a sphere of radius $2k_0^{ext}$. θ is truncated between 45°and 135°to avoid taking into account degradated plane waves.

As a result of Born approximation, a residual frequency variation with respect to the frequency and depending on the size and permittivity of the object appears. This produces a destructive interference when adding coherently multi-frequency images. As explained in [7], by combining only the magnitude of the images, the algorithm is applicable and preserves the shape and size of reconstructed objects.

III. Numerical Results

In this section, the assessment of the algorithm is accomplished by using computer simulations of simplified 3D breast phantoms. Two different scenarios are considered: isolated and body attached simplified breast phantoms. Both scenarios consist of homogeneous low-adipose breast tissue with the inclusion of a tumoral tissue modeled as a sphere of high permittivity.

In this first 3D imaging attempt, permittivity values have been scaled, see Table I. In this way, air can be used as external medium without significant permittivity mismatching regarding the body under test, as done in the experimental measurements included in next section. The scanning system consists of both transmitters and receivers placed along the surface of a cylinder of 22 cm in diameter, composed by 25 rings of 32 antennas separated 1 cm in z direction, as shown in Fig. 1. UWB frequencies (3.1 - 10.6 GHz) have been used as illumination signal for its good compromise between penetration and resolution.

TABLE I
Dielectric properties of the phantom constituents

Tissue	Material	ϵ_r	Contrast
Matching medium	Air	1	-
Breast	Paraffin	2.19	0.54
Tumor	Plasticine	5	0.56

A. Isolated spherical simplified breast phantom

A first scenario consists of an isolated centered sphere with a spheric off-centered tumor inserted, see Fig. 4. With this canonical scenario we will demonstrate the appropriateness of developing a 3D imaging system to provide a reliable detection of unknown masses. This is not possible when using a 2D algorithm, due to its incapacity to discriminate vertically. Accordingly, when reconstructing a real 3D breast using a 2D algorithm, any localized inhomogeneity (nipple, fibro-glandular tissue, etc.) may produce a disturbance which may be visible in all the vertical cuts, independently on the height, that may mask possible tumors. In Fig. 5(a) the reconstruction of the first scenario using the 2D version of the algorithm is presented. Although the tumor is placed at $(20, 10, 10)mm$, the reconstruction of a cut corresponding to the plane $z = 0$ (no tumor) shows reminiscences of the tumor and presents many artifacts. On the other hand, if the same cut is plotted using 3D algorithm, the tumor is not visible, as expected, see Fig. 5(b). Fig. 6 shows the 3 orthogonal planes intersecting at the tumor for the 3D reconstruction. This states the capability of the 3D algorithm to provide vertical discrimination and localize precisely the tumor. In Fig. 7 the 3D reconstruction of a healthy breast phantom is presented to demonstrate the capacity of the algorithm to reconstruct bodies without artifacts that could be misinterpreted as tumors.

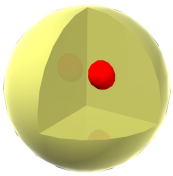

Fig. 4. Isolated spherical simplified breast phantom.

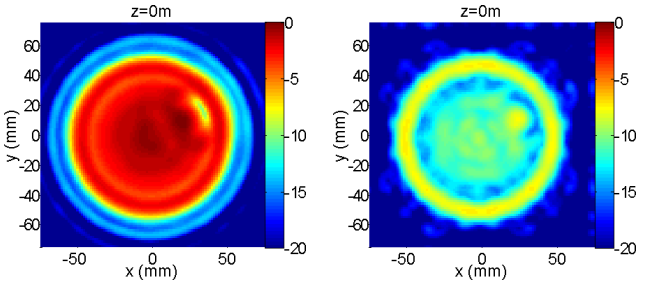

(a) 2D reconstruction.

(b) Horizontal cut of the 3D reconstruction.

Fig. 5. UWB reconstruction of a isolated spherical breast phantom with a tumor inserted. 2D reconstruction and 3D cut of plane $z = 0$.

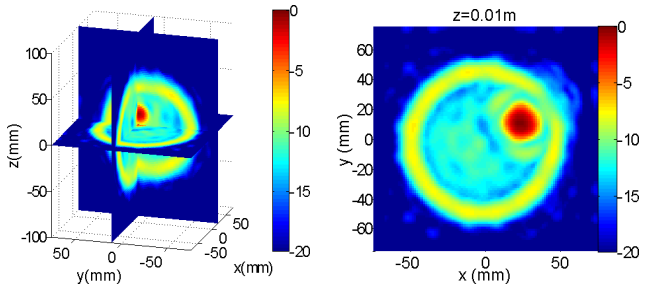

(a) 3D reconstruction. (b) Horizontal cut corresponding to the position of the tumor.

Fig. 6. 3D UWB reconstruction of a isolated spherical breast phantom with a tumor inserted.

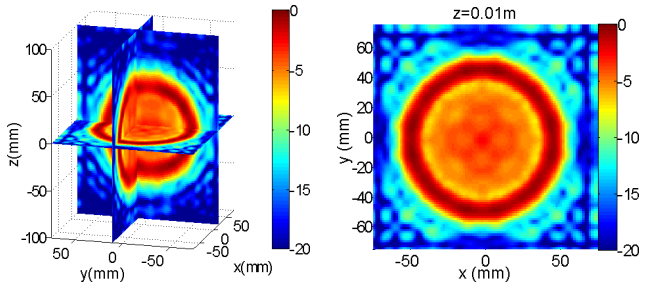

(a) 3D reconstruction. (b) Horizontal cut.

Fig. 7. 3D UWB reconstruction of a isolated spherical healthy breast phantom.

B. Body attached semi-spherical simplified breast phantom

The second scenario constitutes a more realistic simulation. The breast is modeled as a semi-spherical phantom and includes the chest wall. In this case the extent of the probes is truncated by the chest, which also produces more undesired reflections. As can be seen in Fig. 9 the algorithm is able to retrieve both the shape and size of the breast. The tumor is also detected but due to the truncation of the cylindrical antenna, the vertical discrimination gets worst.

Fig. 8. Body attached semi-spherical simplified breast phantom.

IV. Experimental Results

An embryonic imaging system setup able to provide measurements on a cylinder is presented in this section. At the current stage of development, the object under test cannot be immersed in any medium apart from air. This poses limitation to the permittivities of the breast phantom constituents, since high contrasts between two consecutive mediums produce high undesired reflections. Thus, scaled permittivity values have been used, allowing to employ widely available materials to build the phantoms.

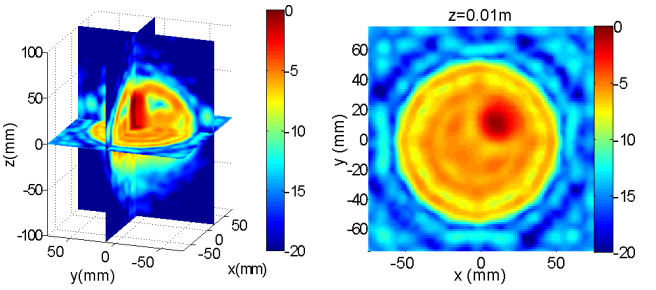

(a) 3D reconstruction. (b) Horizontal cut corresponding to the position of the tumor.

Fig. 9. 3D UWB reconstruction of a body attached spherical breast phantom with a tumor inserted.

A. Measurement Setup

Experimental results are obtained by means of the measurement setup presented in Fig. 10. It consists of 2 antennas, a network analyzer as a receiver, a computer to control remotely the measurement procedure and the positioning system. In order to acquire experimental data of a general body on a cylinder, 4 degrees of freedom are usually needed. However, to simplify the setup, only phantoms with revolution symmetry have been taken into account. In this case, the measurement can be performed by using 2 linear positioners and a rotary stage. A linear positioner is used to move the breast phantom upwards and downwards, the rotary stage confers the rotation on one antenna, while the other antenna moves upwards and downwards thanks to the other linear positioner. The remaining measurements can be obtained by taking advantage of the system symmetry.

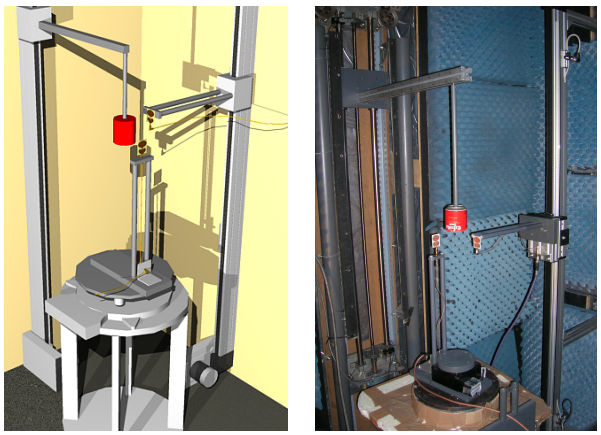

(a) Artist view of the measurement setup. (b) Photo of the measurement setup.

Fig. 10. The experimental setup consists of 2 UWB antennas one of them on a rotor and the other one on a linear positioner. Another linear positioner confers movement to the object under test.

B. Preliminary measurements

Preliminary experimental measurement efforts are made using a centered cylinder of aluminium of 65 mm in diameter and 70 mm in heigh as object under test. Two successive

measurements have been done, in presence and absence of the object, to retrieve the scattered fields.

Fig. 11 shows the results of the 3D reconstruction corresponding to the measured data. As can be seen the contour of the object is well reconstructed preserving both shape and size.

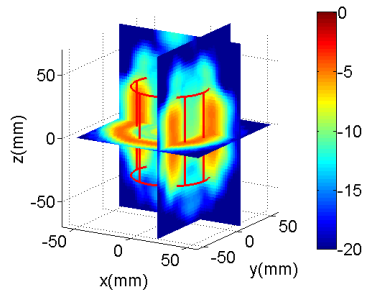

Fig. 11. 3D UWB reconstruction of a centered aluminium sphere from experimental measurements.

V. Conclusions

In this paper a novel 3D UWB tomographic algorithm for breast cancer detection has been presented and assessed. For its validation a 3D simplified cancerous breast model has been simulated and manufactured in order to show the robustness of the algorithm to both numerical and preliminary experimental data. While 2D reconstructions are unable to distinguish between features at different heights, 3D reconstructions allow to obtain a complete localization of the body under test and thus, allow to differentiate malignancy to other usual breast inhomogeneities.

A cylindrical measurement system with 3 degrees of freedom (1 rotation and 2 linear) has been built in order to scan objects with revolution symmetry. First reconstructions of experimental data have shown encouraging results.

Acknowledgment

This work was supported in part by the Spanish Interministerial Commission on Science and Technology (CICYT) under projects TEC2007-66698-C04-01/TCM and CONSOLIDER CSD2008-00068 and by Ministerio de Educación y Ciencia through the FPU fellowship program.

References

[1] J. Ferlay, P. Autier, M. Boniol, M. Heanue, M. Colombet, and P. Boyle, "Estimates of the cancer incidence and mortality in europe in 2006," *Annals of Oncology*, vol. 8 (3), pp. 581–592, 2007.

[2] M. Lazebnik, L. McCartney, P. D., C. B. Watkins, M. J. Lindstrom, J. Harter, S. Sewall, A. Magliocco, J. H. Booske, M. Okoniewski, and S. C. Hagness, "A large-scale study of the ultrawideband microwave dielectric properties of normal, benign and malignant breast tissues obtained from cancer surgeries," *Phys. Med. Biol.*, vol. 52, no. 20, pp. 6093–5115, 2007.

[3] J. Rius, C. Pichot, L. Jofre, J. Bolomey, N. Joachimowicz, A. Broquetas, and M. Ferrando, "Planar and cylindrical active microwave temperature imaging: numerical simulations," *Medical Imaging, IEEE Transactions on*, vol. 11, no. 4, pp. 457–469, Dec 1992.

[4] S. Hagness, A. Taflove, and J. Bridges, "Two-dimensional fdtd analysis of a pulsed microwave confocal system for breast cancer detection: fixed-focus and antenna-array sensors," *Biomedical Engineering, IEEE Transactions on*, vol. 45, no. 12, pp. 1470–1479, Dec. 1998.

[5] R. Kruger, W. Kiser, D. Reinecke, G. Kruger, and R. Eisenhart, "Thermoacoustic computed tomography of the breast at 434 mhz," in *Microwave Symposium Digest, 1999 IEEE MTT-S International*, vol. 2, 1999, pp. 591–594 vol.2.

[6] A. Fhager and M. Persson, "Using a priori data to improve the reconstruction of small objects in microwave tomography," *Microwave Theory and Techniques, IEEE Transactions on*, vol. 55, no. 11, pp. 2454–2462, Nov. 2007.

[7] M. Guardiola, S. Capdevila, and L. Jofre, "Uwb bifocusing tomography for breast tumor detection," in *Antennas and Propagation, 2009. EuCAP 2009. 3rd European Conference on*, March 2009, pp. 1855–1859.

[8] M. Guardiola, S. Capdevila, S. Blanch, J. Romeu, and L. Jofre, "Uwb high-contrast robust tomographic imaging for medical applications," in *Electromagnetics in Advanced Applications, 2009. ICEAA '09. International Conference on*, Sept. 2009, pp. 560–563.

[9] J. De Zaeytijd, A. Franchois, C. Eyraud, and J.-M. Geffrin, "Full-wave three-dimensional microwave imaging with a regularized gaussnewton method theory and experiment," *Antennas and Propagation, IEEE Transactions on*, vol. 55, no. 11, pp. 3279–3292, Nov. 2007.

[10] M. Klemm, J. A. Leendertz, D. Gibbins, I. J. Craddock, A. Preece, and R. Benjamin, "Microwave radar-based breast cancer detection: Imaging in inhomogeneous breast phantoms," *Antennas and Wireless Propagation Letters, IEEE*, vol. 8, pp. 1349–1352, 2009.

[11] N. Joachimowicz, C. Pichot, and J. Hugonin, "Inverse scattering: an iterative numerical method for electromagnetic imaging," *Antennas and Propagation, IEEE Transactions on*, vol. 39, no. 12, pp. 1742–1753, Dec 1991.

[12] S. Semenov, A. Bulyshev, A. Souvorov, A. Nazarov, Y. Sizov, R. Svenson, V. Posukh, A. Pavlovsky, P. Repin, and G. Tatsis, "Three-dimensional microwave tomography: experimental imaging of phantoms and biological objects," *Microwave Theory and Techniques, IEEE Transactions on*, vol. 48, no. 6, pp. 1071–1074, Jun 2000.

[13] M. Ali and M. Moghaddam, "3d nonlinear time-domain inversion technique for medical imaging," in *Antennas and Propagation Society International Symposium, 2008. AP-S 2008. IEEE*, July 2008, pp. 1–4.

[14] A. Abubakar, P. van den Berg, and J. Mallorqui, "Imaging of biomedical data using a multiplicative regularized contrast source inversion method," *Microwave Theory and Techniques, IEEE Transactions on*, vol. 50, no. 7, pp. 1761–1771, Jul 2002.

[15] J. Johnson, T. Takenaka, K. Ping, S. Honda, and T. Tanaka, "Advances in the 3-d forwardbackward time-stepping (fbts) inverse scattering technique for breast cancer detection," *Biomedical Engineering, IEEE Transactions on*, vol. 56, no. 9, pp. 2232–2243, Sept. 2009.

[16] J. Romeu and L. Jofre, "Truncation errors in cylindrical near to far field transform. a plane wave synthesis approach," in *Microwave Conference, 1992. 22nd European*, vol. 1, Sept. 1992, pp. 659–663.